The Impact of Heat Storage Material Integration in an Evacuated Tube Collector

C. Rajasekar[1*], R. Rameshkumar[2], R. Barathiraja[3]

[1]Department of Mechatronics Engineering, Akshaya College of Engineering and Technology, Kinathukadavu, Coimbatore – 642109, Tamil Nadu, India

[2]Department of Mechanical Engineering, Builders Engineering College, Tirupur – 638108, Tamil Nadu, India

[3]Department of Mechanical Engineering, Mahakavi Bharathiyar College of Engineering & Technology, Vasudevanallur,s Tirunelveli -627758, Tamil Nadu, India

Received 24.10.2024.

Revised 22.5.2025.

Accepted 5.6.2025.

https://doi.org/10.2298/CICEQ241024014R

*Corresponding Author: Email id: - rajasekarmech006@gmail.com , Mobile no +91 9843385166

ABSTRACT

This experimental research assessed the impacts of sensible and latent heat materials such as SAE 20W/40 (used engine oil), candelilla wax (CLW) and rice bran wax (RBW) in an evacuated tube solar air heater. Four distinct arrangements were studied: one without a thermal energy storage material (TESM), one with a sensible heat material (SHM), and two with latent heat materials (LHM), to enable comparative analysis. The maximum outlet temperature of air for ETC filled with engine oil was 108°C, for CLW 115°C and for RBW 133°C – all measured at 13:00 pm. However, without filling the TESM in the ETC, the outlet temperature was only 70 °C. The maximum temperature difference of air in the RBW material-filled ETSAH system was 94°C, whereas without TESM, the temperature was only 31°C at 13:00. The maximum efficiency of the ETSAH system was achieved when using RBW as a PCM rather than both CLW and used engine oil-filled TESM. Moreover, the efficiency of the system increases around 1.7 - 1.8 times when the velocity of air increases from 1.5 to 2.5 m/s.

Key words*:* Evacuated tube collector; Latent Heat; Sensible Heat; Thermal storage material; Rice bran wax; Candellila wax

List of Symbols and Abbreviations

α	-	Absorptance of inner surface of evacuated tube collector
CLW	-	Candelilla Wax
DSC		Differential scanning calorimeter
Q_c	-	Energy incident on the collector tube ,Watts
Q_f	-	Energy absorbed by air, Watts
η_c	-	Evacuated tube solar air heater efficiency
ETC	-	Evacuated Tube Collector
ETSAH	-	Evacuated Tube Solar Air Heater
HTF	-	Heat Transfer Fluid
T_{in}	-	Inlet temperature of air, ^{0}C
S.I	-	Intensity of solar radiation , W/m^2
LHSM		Latent Heat Storage Material
m_a	-	Mass flow rate of air, kg/s
T_{out}	-	Outlet temperature of air, ^{0}C
PCM	-	Phase Change Materials
A_p	-	Projected area of evacuated tube solar air collector tube exposed to the sun light, m^2
RBW	-	Rice Bran Wax
SHSM	-	Sensible Heat Storage Material
SAE	-	Society of Automotive Engineering
SAH	-	Solar Air Heater
C_{pa}	-	Specific heat of air, J/kg.K
ΔT	-	Temperature difference , ^{0}C
ΔT_{CLW}	-	Temperature difference with Candelilla Wax, ^{0}C

ΔT_{RBW}	-	Temperature difference with Rice Bran Wax, ^0C
ΔT_{oil}	-	Temperature difference with Used Engine oil, ^0C
ΔT_{wo}	-	Temperature difference without use of thermal energy storage materials, ^0C
T_{CLW}	-	Outlet air Temperature with Candelilla Wax, ^0C
T_{RBW}	-	Outlet air Temperature with Rice Bran Wax, ^0C
T_{oil}	-	Outlet air Temperature with Used Engine oil, ^0C
T_{wo}	-	Outlet air Temperature without use of thermal energy storage materials, ^0C
TESM	-	Thermal Energy Storage Materials
η_{CLW}	-	Thermal efficiency with Candelilla Wax
η_{RBW}	-	Thermal efficiency with Rice Bran Wax
η_{oil}	-	Thermal efficiency with Used Engine oil
$\eta_{w.o}$	-	Thermal efficiency of without use of thermal energy storage materials
τ	-	Transmittance of the collector tube
Q_u	-	Useful energy gained from the collector (W)
20W/40	-	20 W- operating range at cold temperatures & 40 -operating range at high temperature

INTRODUCTION

The demand for traditional energy resources is now incredibly high, as non-renewable energy sources are continually exhausted every day. The development of technology like renewable energy sources is essential in the future to keep global energy supplies steady. Non-conventional energy sources, such as solar, play a pivotal role in energy production, as non-renewable energy sources are constantly declining. Solar energy is an optimistic and plentiful option. In many applications, solar energy is both environmentally sustainable and energy-saving. Solar energy can be used very effectively to generate hot air to substitute electric heaters

for industrial and space heating applications, electricity generation, refrigeration and air conditioning, and drying of food products [1-4].

Solar heat energy, owing to its clean nature and abundant availability, has been preferred over other promising renewable energy sources [5-7]. Solar energy is an intermittent resource of energy. However, it mainly depends on environmental conditions and is also a time-dependent supply source. The simplest and most commonly accepted approach is to convert solar energy into a potential heat resource [8-10].

In any method for harvesting solar heat energy, the solar collector is a primary device of such a system. The solar power is collected by the solar collector and is converted into heat, and the heat energy is transferred into the heat-gaining fluid, like air or water that commonly flows through the system. Indeed, solar heating is an ancient technique; nevertheless, progressive technologies have emerged consistently to enhance solar absorption and output temperature. According to Tyagi et al. [11], thermal energy storage systems are a key element in the energy harvesting approaches as well as pronounced techniques, especially in solar energy-storing systems.

Heat energy coming from sun is collected by various types of solar collectors, like flat plate collectors (FPC), evacuated tube collectors (ETC), and concentrating detectors, with flat plate collectors often used for low-temperature needs. Moreover, the ETC works at higher fluid outlet temperatures, which is required; however, it has a high cost and has a longer payback period compared to FPC [12]. Evacuated tubes have had heated water for years, but not air in commercial settings. Across the globe, people utilise one-ended glass evacuated tubes for their enhanced efficiency. ETC, rather than FPC, achieved the high temperature of the outlet air under the same atmospheric conditions [13-14].

In general, the potential heat source can be reserved in the form of sensible heat, latent heat, or chemical energy [9, 15]. Latent heat storage (LHS) systems using phase-change materials (PCM) are preferred methods because they can store more energy and keep heat at stable temperatures during the melting process [16-18]. Phase change materials can be classified as organic, artificial, and eutectic. Organic PCMs include paraffin waxes and fatty acids that are biologically stable, don't corrode, and works at high temperatures. However, their heat conduction properties are not good, and they can catch fire easily. Inorganic PCMs, such as salt hydrates and some metals, have the capability of holding more latent heat and transferring heat more efficiently than biological PCMs. But these PCMs have problems like supercooling, phase separation, and corrosion, though, and usually need stabilisers or sealing methods to fix. Eutectic PCMs are mixes that melt and harden at a single, clear temperature. Organic and inorganic materials, or organic and inorganic materials, can be mixed together as per the requirement. This gives the freezing point that is required. Eutectics are good because they have a sharp phase change temperature and can be designed in a lot of different ways, but they can be more expensive and may not be stable over long periods of thermal cycles. Different types of PCM are picked based on the application's temperature needs and limitations [24, 25]. Low thermal conductivity is a problem that phase change materials (PCMs) often have. Several enhancement methods are used to get around this problem. Additives with high conductivity are often used. These can be metal nanoparticles (like Al, Cu, and Ag) or carbon-based materials such as graphene, carbon nanotubes (CNTs), and expanded graphite (EG). These additives make electrical paths inside the PCM, which speeds up the flow of heat. Adding metal foams or structures with fins to the PCM is another way to make it easier for heat to move through. The methods of microencapsulation and nanoencapsulation also help to improve thermal conductivity while keeping the structure stable. Moreover, form-stable hybrid PCMs are created by adding PCMs to porous, heat-conducting materials like metal oxides or graphite. These

methods not only improve the flow of heat, but they also make PCMs more reliable and stable over time in real-world situations. In addition to changes in composition, adding thermally conductive materials and changing the geometry or shape of the inserts are very important for making PCMs better at conducting heat. In order to improve the effective heat transfer area and speed up thermal response, metallic inserts made of copper, aluminium, or stainless steel are often built into the PCM. These inserts can be in the form of pins, rods, fins, wires, or mesh structures [26-30]

If SAH system integrated with PCM is used enormous heat can be stored rather than sensible heat storage (SHS) system. Advanced PCMs are applied extensively in LHS system and solid – liquid PCMs materials for storing thermal energy resources approximately 5 to 14 folds more than SHS systems [19-22]. So, it is a desirable choice if the supply and demand of heat energy resources is inconsistent and is ideal for solar air heating system due to excellent thermal efficiency behaviour [11, 21].

Tyagi et al. [11] experimentally analysed that the ETC-type solar air heater integrated with and without SHM and PCM. The efficiencies of heat storage medium is substantially higher in comparison to that without energy storage materials and also the efficiencies of PCM are remarkably greater than that of SHM and without arrangements. Similarly, an ETC- solar air heater experimentally investigated by Kumar et al.[10], in which the performance of the system was analysed by varying the inlet air flow rates as well as with and without assistance of reflector. The results indicated that the highest outlet temperature and peak differential air temperature of 97.4 ^{0}C and 74.4 ^{0}C were obtained when air flow on the system of 6.70 kg per hours. Khadraoui et al. [6] examined the solar air heater (SAH) integrated with and without PCM. It is reported that the efficiency of the SAH integrated with PCM achieved as 33% whereas without energy storage arrangement reached only 17%. Similarly, Jain et al. [23] claim

that the LHS material performs greater than SHS materials in which the myristic acid was utilised as PCM.

According to the comprehensive literature review, many studies have been conducted on solar air heaters integrated with both sensible and latent heat storage materials. However, no experimental study has yet investigated an evacuated tube solar air heater (ETSAH) integrated with thermal energy storage materials such as Candelilla wax, Rice bran wax, and used engine oil of SAE 20W/40. Keeping this gap in mind, the present investigation aims to examine the thermal performance—specifically the outlet temperature, temperature difference of the working fluid, and system efficiency during both sunshine and post-sunset periods under Indian climatic conditions. Additionally, the study evaluates the effect of varying air flow rates in a solar air heater (SAH) integrated with a thermal energy storage unit compared to a system without thermal energy storage materials. Furthermore, the use of thermally active organic materials like waxes and used engine oil in the evacuated tube, along with the thermal interaction between the heat transfer fluid and the storage medium, inherently contributes to enhancing the effective thermal conductivity (k) of the system, thereby improving the overall heat transfer performance.

2. MATERIAL AND METHODS

2.1 MATERIALS

Four experimental studies have been carried out: one without any thermal energy storage materials (TESM), one with sensible heat storage material (SHSM), and two with latent heat storage materials (LHSM). An ETC acts as a solar air heater in these experiments, and a total of four frames have been designed, in which each frame has five tubes. The copper pipe, 10 mm in diameter, is placed inside of the evacuated tube through a U-bend to move air freely inside of the tube. One inlet manifold which is made of PVC and has a diameter of 150 mm, used to supply the working fluid into all setups with the help of one blower. The inlet manifold and inlet of the copper tube of each setup were connected by four different lengths of plastic hoses (1000mm,

1500mm, 2000 mm, and 2500 mm). The description of the ETC details and sensible heat storage material (SHSM) were illustrated in **Table 1.**

Inert Table 1

The ETC frame does not contain any heat storage materials. The second arrangement of the ETC frame contains 11 litres (2.2 litres each) of used engine oil (SAE-20W/40), and it acts as a sensible heat storage material (SHSM). The third and fourth setups are filled with bio-phase change materials (PCMs), including 10 kg of rice bran wax (RBW) and 10 kg of candillia wax (CLW), which is latent heat storage materials (LHSM).

2.2 EXPERIMENT SET-UP

For four arrangements and three different flow rates experiments were carried out on evacuated tube collectors with and without TESM. A total of 20 ETC tubes were used in this analysis, in which 5 were filled with RBW, 5 with CLW, 5 with engine oil, and another 5 empty tubes, all placed in series. **Fig. 1 (a, b & c)** shows the full illustration of a dual-wall type evacuated tube made of glass, inside which the TES is kept.

Inert Figure 1

One frame contains five tubes of ETC, which are used to absorb the radiated heat from the sun. The absorption takes place as heat absorption coating is applied on the surface of the tube. The frame is set at an angle of 40^0 from the ground to absorb sun radiation. In this process, two types of PCMs are used to absorb the thermal energy as explained above, and their properties are listed in **Table 2.**

Inert Table 2

Inert Figure 2

In this set up, the heated air temperature was measured by 17 thermocouples (RTD PT100) in which one is placed in the inlet of the system, to measure the inlet air temperature, four placed in the exit condition and 12 placed inside the 3-collector tubes (TESM) for each frame (1, 3 and 5).The copper tubes are connected in series, that is, the outlet of the first tube is connected with the inlet of the second tube and the rest of the tubes are connected similarly. The hot wire anemometer is used to find the velocity of the air and it is placed between the inlet of the manifold and ETC frames. The pressurized air is circulated in to the system by using an air blower and solar intensity is measured for every half an hour using solar power meter.

2.3 MEASURING DEVICES AND INSTRUMENTS

An RTD PT100 temperature sensor, together with a digital temperature indicator, was employed to precisely measure the temperature range, which varies from 0°C to 200°C with an accuracy of ± 0.5°C and a resolution of 0.10°C. The fluid velocity is monitored using a digital hot wire anemometer (Lutron AM-4204), whose measuring accuracy (± 5 % + 1 d) and resolution are ± 0.1 m/s. The solar power during daylight hours was measured using a solar power meter (Model – CEM DT 1307), and the device offers an accuracy of ±10 W/m² and a resolution of 1 W/m². The phase change material properties were determined by Differential Scanning Calorimeter-DSC 6000 (PerkinElmer). DSC test results for the PCM in conditions between 0°C and 100°C for the heating interval and 5°C/min for the heating rate are given in Fig**. 2 (a & b).** Thermal conductivity and specific heat of latent heat materials were determined by the Thermal Properties Analyser (Model-KD2 Pro), and its range is from 0.02 to 2.00 W/m.K, and accuracy is ±5% from 0.2 to 2 W/m.K ± 0.01 W/m.K from 0.02 to 0.2 W/m.K.

2.4 EXPERIMENTAL PROCEDURE

In this system, the Sensible and Bio-PCMs were placed inside the ETC device without adding any TESM, and the ETC was heated by radiation from solar energy. Heat storage

materials are used to prevent fluctuations in outlet air temperature due to atmospheric variations. The TESM absorbs and stores the heat energy, transferring some of it to the heat-carrying fluid. The stored energy of sensible and latent heat was utilised when the sunshine was low or at night. In order to confirm the repeatability of the analysis, three studies were conducted for every test on different days of the same month. A centrifugal blower sucks atmospheric air, an anemometer measures it, and a gate valve is used for controlling it. The specified forced air acts as a heat-carrying fluid, and it passes through the hollow copper tube in the ETSAH of all four arrangements at the same time. The temperature of the inlet air is measured before it enters the first tube, as mentioned in the experimental setup procedure. The three different air flow velocities of 1.5, 2.0, and 2.5 m/s were carried out, and their impacts were analysed. The experimental data was collected from the system over a few days in the month of April by varying the velocity of air. The temperature deviations of the working fluid and the efficiency of ETSAH with and without TESM were evaluated during the period.

2.5 UNCERTAINTY ANALYSIS

An errors in the investigations would arise from measuring instrument, weather condition specified space condition, inspection and records due to uncertainities. In the present experimental investigations, the uncertainties involved in the measurement of temperature, velocity of air and solar intensity have been measured through the appropriate instruments and are listed in **Table 2.** The computed value M is a function of several independent parameters x_1, x_2, x_3 ...x_n

$$M = M(x_1, x_2, x_3 \ldots x_n)$$

The total uncertainty in the assessment of M is computed from the method suggested by Senthil [8]

$$\delta M = \left[\left(\frac{\partial M}{\partial x_1} \delta x_1 \right) + \left(\frac{\partial M}{\partial x_2} \delta x_2 \right)^2 \cdots\cdots\cdots \left(\frac{\partial M}{\partial x_n} \delta x_n \right)^2 \right]^{\frac{1}{2}} \quad (1)$$

Let δM is the uncertainty in the result of δx_1, δx_2, δx_3..... δxn. The uncertainties in the estimation of overall ETSAH system is 2.8% to 5.2%.

Inert Table 2

2.6 ENERGY ANALYSIS

Energy analysis is an essential component in evaluating the performance and efficiency of any thermal system. Based on the first law of thermodynamics, it involves quantifying the energy input, transformation, and output. In solar thermal systems, energy analysis focuses on the conversion of incident solar radiation into usable thermal energy. This process is influenced by factors such as the intensity and wavelength range of the solar radiation. The efficiency of this conversion depends on how effectively the system captures and utilizes the available energy. For an evacuated tube collector (ETC), the incident radiation energy is represented and analyzed as follows [11, 14].

$$Q_c = AS.I \quad (2)$$

Useful energy earned from collector it may be expressed in the following way [10, 11]:

$$Q_u = \alpha \tau S.IA \quad (3)$$

The useful energy transmitted into the ETC and is harvested by heat carrying fluid (air) and was computed with the help of the following energy equation;

$$Q_f = m_a C_p \Delta T \quad (4)$$

The efficiency of ETSAH system is described as the ratio between the heat energy acquired by heat carrying fluid to heat energy strike on ETC and is expressed by [11]

$$\eta_c = Q_f / Q_c = m_a C_p \Delta T / AS.I \quad (5)$$

3. RESULTS AND DISCUSSION

In this research work, the effect of the three different air velocities flowing through the ETSAH system, with and without TESM, is studied. During the month of April 2024, the tests were performed under almost similar conditions on different days when the sky was almost clear. During the test-conducted days, the air temperature varied from 26 to 36 °C. The tests were conducted between 10:00 and 21:00, and data was collected for every half an hour. Three different studies were analysed, such as (i) evacuated tube solar air heater at low air velocity, (ii) evacuated tube solar air heater at medium air velocity, and (iii) evacuated tube solar air heater at high air velocity.

3.1 Performances analysis of the ETSAH system at an airflow velocity of 1.5 m/s

The measurements were taken initially before the ETSAH system was exposed to solar radiation also after exposing to solar radiation. The impact of a low airflow velocity (1.5 m/s) of the thermal energy-carrying fluid on the ETSAH system, both with and without TESM, is depicted in Fig. 3(a) and (b). These graphs illustrate the variations in inlet and outlet air temperatures, the temperature difference, and the solar radiation over time. The peak solar radiation recorded was 1004 W/m² at 13:00 p.m as well as the solar intensity values of approximately 810–830 W/m² and an inlet air temperature of around 31°C were consistently observed at 9:00 a.m., as shown in Figure 3(a) and also referenced in Figure 3(b).

.

Inert Figure 3

Shortly after midday, the maximum solar irradiance began to decline. In the ETSAH system, the outlet air temperature and the air temperature difference strongly depend on both the incident solar radiation and the air velocity. Due to the high solar absorption capacity of the evacuated tube collector (ETC) and the relatively low air velocity (1.5 m/s), the residence time of air inside the collector is longer, allowing greater heat transfer to the fluid. Consequently, the outlet temperature increased substantially above ambient levels.

Based on the experimental results, the outlet air temperatures observed at 9:00 a.m. were approximately 43°C, 49°C, 51°C, and 56°C for the cases with no thermal energy storage material (TESM), Engine Oil, CLW, and Rice Bran Wax (RBW), respectively. Furthermore, after 16:00 p.m., as solar intensity declined, the temperature difference also started to decrease. From the experimental results, without any TESM in the ETC, the maximum inlet and outlet air temperatures reached 37 °C and 66 °C at 13:00 p.m. However, when filled with TESMs, the maximum outlet air temperatures increased to 95 °C (engine oil), 104 °C (CLW), and 119 °C (RBW) respectively at the same time. This enhancement is attributed to the thermal energy storage capability of the TESMs, especially the latent heat storage in CLW and RBW, which allows for the storage of solar heat during peak radiation and its release during lower radiation periods.

In ETCs filled with sensible heat material (engine oil), the maximum differential temperature achieved was 58 °C, while those filled with latent heat materials (CLW and RBW) achieved 67 °C and 82 °C respectively. In contrast, the system without TESM only achieved a 29 °C temperature difference. These results demonstrate that latent heat materials offer superior thermal buffering, maintaining higher outlet temperatures even as solar intensity fluctuates, due to their phase change properties, which absorb and release heat at nearly constant temperatures.

Figure 3(b) presents the system's efficiency variation over time. At an airflow velocity of 1.5 m/s, the efficiency of the system increased slightly up to 13:30 p.m. This is because the temperature difference between inlet and outlet air, which drives thermal energy gain, was increasing more significantly than the decline in solar irradiance. From 13:30 to 16:00 p.m., the efficiency remained relatively constant as both temperature differential and solar radiation balanced out. However, between 16:00 and 17:00 p.m., the efficiency increased sharply, despite decreasing solar intensity. The outlet air temperature is higher for collectors with thermal energy storage materials (TESMs), particularly with Rice Bran Wax (RBW) and Candelilla Wax (CLW) compared to that without TESM. This is due to high thermal conductivity and high latent heat properties and gradual thermal discharge behaviour of the phase change materials, which prolong heat retention and enhance outlet temperatures during both low and moderate radiation periods [31, 32].

The maximum system efficiency recorded at 17:30 p.m. was: 9.8% without TESM, 36.7% with used engine oil, 42% with CLW, and 54.6% with RBW. This confirms that RBW, due to its higher latent heat capacity and effective phase transition temperature, is more effective at storing and releasing heat, thereby maintaining system output during declining solar periods. The higher thermal conductivity and better heat transfer characteristics of RBW also contribute to this superior performance. In summary, the experimental findings confirm that system efficiency is directly proportional to the temperature differential of the heat transfer fluid and inversely proportional to instantaneous solar intensity—a trend also reported in earlier studies on ETSAH systems at various mass flow rates [5, 11, 14].

3.2 Performances analysis of the ETSAH system at an airflow velocity of 2.0 m/s

The effect of a moderate airflow velocity (2.0 m/s) of the heat-carrying fluid in the ETSAH system, both with and without thermal energy storage materials (TESMs), is shown in

Fig. 4(a) and (b). The graphs illustrate variations in inlet and outlet air temperatures, the corresponding temperature differences, and solar radiation over time. The maximum solar radiation was recorded at 1010 W/m² at 13:00 p.m. As expected, the solar intensity began to decline in the early afternoon due to the natural daily solar cycle.

Inert Figure 4

Given the high absorptivity of the evacuated tube collector (ETC) and the increased velocity of the air stream (2.0 m/s), the outlet air temperature rose significantly above the ambient temperature. This is because the higher velocity enhances the convective heat transfer coefficient, promoting more effective energy exchange between the heated ETC surface and the passing air. Although higher velocities reduce the residence time of air within the tubes, the increased turbulence leads to improved heat pickup from the collector surface.

From the experimental data, without any TESM, the maximum inlet and outlet air temperatures were 39 °C and 66.5 °C respectively at 13:00 p.m. In contrast, the ETSAH filled with TESMs reached maximum outlet temperatures of 103 °C (engine oil), 113 °C (CLW), and 130 °C (RBW), as shown in Fig. 4(a). This substantial improvement is attributed to the thermal buffering effect of TESMs, particularly those with latent heat storage (CLW and RBW), which can absorb excess solar energy during peak irradiance and release it gradually over time.

The maximum differential air temperatures achieved were: 27.5 °C without TESM, 64 °C with engine oil (sensible heat storage), 74 °C with CLW, and 91 °C with RBW. These results reinforce the superior performance of latent heat TESMs, as they provide higher energy density storage and a near-isothermal heat absorption/release process, which stabilizes and extends heat delivery to the working fluid. Additionally, the increase in airflow velocity from 1.5 to 2.0 m/s contributed to rise in outlet temperature and air temperature difference. This improvement is due to the enhancement of the heat transfer rate at higher mass flow rates. Although higher velocity

can reduce air residence time, the effect is compensated by the increased mass flow rate and convective heat exchange due to a thinner thermal boundary layer.

Figure 4(b) displays the system efficiency and solar radiation intensity over time at the 2.0 m/s inlet velocity. Initially, system efficiency increased slightly up to 13:00 p.m., as the temperature difference dominated over changes in solar input. From 13:30 to 16:00 p.m., the efficiency trend remained relatively flat. However, after 16:00 p.m., the system efficiency surged significantly. This is because TESMs, especially phase change materials (PCMs), released previously stored heat during the declining solar phase, decoupling the system's thermal output from immediate solar input.

The maximum system efficiencies recorded at 17:30 p.m. were: 12.3% without TESM, 49.2% with used engine oil, 57.8% with CLW, and 71.5% with RBW. The RBW-based Bio-PCM clearly outperformed other TESMs due to its higher latent heat, optimized melting point, and better thermal conductivity, allowing for more efficient charging and discharging cycles. Moreover, increasing the airflow velocity from 1.5 to 2.0 m/s led to an approximate 1.25 to 1.45 times increase in system efficiency across all TESM configurations. This emphasizes the importance of flow rate optimization in enhancing thermal and exergy efficiency in solar air heaters. These findings align with prior studies on ETSAH systems operating at various airflow velocities, where researchers observed a strong correlation between higher airflow rates and improved thermal performance [3, 6, 17].

3.3 Performances analysis of the ETSAH system at an airflow velocity of 2.5 m/s

The effect of a high velocity (2.5 m/s) of the heat-carrying fluid in the ETSAH system with and without thermal energy storage materials (TESMs) is illustrated in Fig. 5(a) and 5(b). These curves demonstrate the variations in inlet and outlet air temperatures, the corresponding temperature differentials, and solar radiation intensity over time. The peak solar radiation was

observed to be 1020 W/m² at 12:30 p.m., followed by a gradual decline in intensity as the afternoon progressed, consistent with the daily solar cycle.

Inert Figure 5

Due to the excellent solar absorption capability of the evacuated tube collector (ETC) surface and the elevated velocity of the airflow, the outlet air temperature significantly exceeded the ambient temperature. Increased airflow enhances the forced convective heat transfer mechanism, which not only improves the heat transfer coefficient but also promotes efficient heat exchange between the inner collector surface and the moving air. While faster airflow reduces the air's residence time inside the tubes, the improvement in turbulence and flow mixing compensates for this, resulting in a higher rate of thermal energy transfer.

From the experimental results: Without any TESM, the maximum inlet and outlet air temperatures were 39 °C and 70 °C, respectively, at 13:00. With TESMs, the maximum outlet temperatures at the same time were 108 °C (Engine Oil), 115 °C (CLW), and 133 °C (RBW), as shown in Fig. 5(a). Among the TESMs, RBW exhibited the highest outlet air temperature due to its high latent heat capacity and better thermal conductivity, which facilitated greater energy storage and release. The maximum differential air temperatures achieved were: 31 °C without TESM, 76 °C with CLW, and 94 °C with RBW.

These results emphasize the superior thermal regulation and heat retention capabilities of PCMs, particularly RBW. The phase change process in RBW enables it to store more thermal energy during periods of high solar intensity and release it steadily even when solar radiation declines.This study clearly shows that increasing the airflow velocity from 1.5 to 2.5 m/s significantly elevates the outlet air temperature and temperature difference. This enhancement is because of the increased convective heat transfer at higher velocities, as described by Newton's law of cooling.

Figure 5(b) displays the system efficiency and solar radiation intensity over time at an inlet velocity of 2.5 m/s. In all cases, system efficiency showed a slight increase up to 13:00 p.m. due to the dominance of temperature rise over the decreasing solar input. From 13:00 to 16:00 p.m., the efficiency curve remained relatively stable. After 16:00 p.m., efficiency increased sharply, attributed to the discharge of previously stored thermal energy by the TESMs, particularly the PCMs, during the period of reduced solar input.

The maximum system efficiencies at 17:30 p.m. were recorded as: 17.2% without TESM, 63.0% with Engine Oil, 66.4% with CLW, and 91.6% with RBW. The system integrated with RBW-PCM consistently achieved the highest efficiency, showcasing the material's capability to utilize both sensible and latent heat modes effectively. Compared to the system without TESM, the efficiency improvements ranged from 67% to 75% when increasing airflow velocity from 1.5 m/s to 2.5 m/s. Similar results have been reported in earlier research works that experimentally analyzed ETC-based solar air heaters under varying airflow rates [11,14], validating the observed trends in thermal performance and efficiency.

Finally, an overall comparison of Figs. 3 to 5 confirms that as the inlet air velocity increases, the thermal efficiency, temperature difference, and outlet air temperature also rise across all cases. This is primarily due to the forced convection heat transfer, which becomes increasingly dominant at higher velocities. Moreover, ETSAH systems integrated with TESMs significantly outperform those without, with RBW standing out as the most effective Bio-PCM due to its favourable thermal storage characteristics and discharge behaviour, especially under variable solar radiation conditions.

4. Conclusions

The experiments conducted have led to the following conclusions:

1. The thermal efficiency of the system, temperature difference and outlet temperatures of air were increased when the velocity of the heat carrying fluid (air) increases from 1.5 to 2.5 m/s.
2. Efficiency of ETC-Solar air heater using rice bran wax (RBW) as a TESM is positively influenced than Engine oil and Candelilla wax and also the efficiency of SAH with all TESMs is observed that can be significantly superior to without TESM.
3. The highest temperature difference of air was attained at higher flow of air velocity 2.5 m/s are 76 ^{0}C and 91 ^{0}C , filled with CLW and RBW in ETSAH, whereas without filled any TESM in ETC was achieved as 31 ^{0}C.
4. The peak efficiency of the system observed as 91.6 % and 17.2 % of filled with RBW-PCM in ETSAH and without filled any TESM respectively, at higher flow of heat carrying fluid velocity 2.5 m/s.
5. The extreme outlet temperature of air has attained at flow velocity of 2.5 m/s, as 66.5 ^{0}C, 108 ^{0}C, 115 ^{0}C and 133 ^{0}C where without filled TESM, filled with Engine oil, CLW and RBW respectively.

Funding: This research received no specific grant from any funding agency in the public, commercial, or not-for-profit sectors

Acknowledgments: The corresponding author wishes to the deepest gratitude to TEQIP-III, New Delhi, and also express the sincere thanks to Department of Mechanical Engineering, Government College of Engineering, Bargur, Krishnagiri, and Tamilnadu.

Conflicts of Interest: The authors declare no conflict of interest.

REFERENCES

1) M. Abuşka, S. Şevik, A. Kayapunar, Appl. Therm. Eng. 148 (2019) 684-693. https://doi.org/10.1016/j.applthermaleng.2018.11.056

2) M. Chaabane, H. Mhiri, P. Bournot, Energy Convers. Manag. 78 (2014) 897-903. https://doi.org/10.1016/j.enconman.2013.07.089

3) K. Chopra, A.K. Pathak, V.V. Tyagi, A.K. Pandey, S. Anand, A. Sari, Energy Convers. Manag. 203 (2020) 112205. https://doi.org/10.1016/j.enconman.2019.112205

4) R. Barathiraja, P. Thirumal, G. Saraswathy, I. Rahamathullah, Chem. Ind. Chem. Eng. Q. 28(3), (2022) 169-178. https://doi.org/10.2298/CICEQ201120028B

5) S.Y. Kee, Y. Munusamy, K.S. Ong, Appl. Therm. Eng. 131 (2018) 455-471. https://doi.org/10.1016/j.applthermaleng.2017.12.032

6) A.E. Khadraoui, S. Bouadila, S. Kooli, A. Guizani, A. Farhat, Appl. Therm. Eng. 107, (2016) 1057–1064. https://doi.org/10.1016/j.applthermaleng.2016.07.004

7) M.M.A. Khan, N.I. Ibrahim, I.M. Mahbubul, H.M. Ali, R. Saidur, F.A. Al-Sulaiman, Sol. Energy. 166 (2018) 334-350. https://doi.org/10.1016/j.solener.2018.03.014

8) R. Senthil, Energy Sources, Part A. 44(1) (2019) 2374-2384. https://doi.org/10.1080/15567036.2019.1649751

9) A. Kumar, S. Kumar, U. Nagar, A. Yadav, J. Sol. Energy. 1 (2013) 524715. https://doi.org/10.1155/2013/524715

10) S. Kumar, A. Kumar, A. Yadav, Int. J. Sustain. Eng. 8 (2014), 280-293. https://doi.org/10.1080/19397038.2013.878001

11) V.V. Tyagi, A.K. Pandey, S.C. Kaushik, S.K. Tyagi, J. Therm. Anal. Calorim. 107 (2012) 1345-1352. https://doi.org/10.1007/s10973-011-1617-3

12) M. Leckner, R. Zmeureanu, Appl. Energy. 88 (2011) 232-241. https://doi.org/10.1016/j.apenergy.2010.07.031

13) P. Manoj Kumar, K. Mylsamy, P.T. Saravanakumar, Energy Sources, Part A. 42 (2020), 2420-2433. https://doi.org/10.1080/15567036.2019.1607942

14) S. Nain, A. Parinam, S. Kajal, Int. J. Ambient Energy. 39 (2017), 143-146. https://doi.org/10.1080/01430750.2016.1269677

15) N.L. Panwar, S.C. Kaushik, S. Kothari, S., Renewable Sustainable Energy Rev. 15 (2011) 1513-1524. https://doi.org/10.1016/j.rser.2010.11.037

16) S. Riffat, B. Mempouo, W. Fang, Int. J. Ambient Energy. 36 (2013) 102-115. https://doi.org/10.1080/01430750.2013.823106

17) A. Sari, A. Karlı, C. Alkan, A. Karaipekli, Energy Sources, Part A. 35 (2013). 1813-1819. https://doi.org/10.1080/15567036.2010.531507

18) S.B. Sasikumar, H. Santhanam, M.M. Noor, M. Devasenan, H.M. Ali, Energy Sources, Part A. (2020)1-13. https://doi.org/10.1080/15567036.2020.1829201

19) D. Singh, P. Mall, Energy Sources, Part A. (2020) 1-18. https://doi.org/10.1080/15567036.2020.1810825

20) A. Yaswanthkumar, V.P. Chandramohan, J. Therm. Anal. Calorim. 136 (2019) 331-343. https://doi.org/10.1007/s10973-018-7756-z

21) L. Liu, R. Wang, Y. Wang, W. Li, J. Sun, Y. Guo, C. Zhao, Energy Convers. Manag. 275 (2023) 116464. https://doi.org/10.1016/j.enconman.2022.116464

22) R.I. Rubel, M.W. Akram, M.M. Alam, A. Nusrat, R. Ahammad, M.A. Al Bari, Arabian J. Sci. Eng. 49 (2024) 14533–14551. https://doi.org/10.1007/s13369-024-09519-z

23) S. Jain, S.K. Dubey, K.R. Kumar, D. Rakshit, (2021) 167-215. https://doi.org/10.1007/978-981-33-6456-1_9

24) N. Ning, C. Sun, Z.J. Ma, S. Guo, S. Jiang, J. Zhang, D. Hou, C. Wang, J. Energy Storage . 114 (2025) 115814. https://doi.org/10.1016/j.est.2025.115814

25) F.L. Rashid, M.A. Al-Obaidi, N.S. Dhaidan, A.K. Hussein, B. Ali, M.B.B. Hamida, O.Younis, J. Energy Storage. 73 (2023) 109219. https://doi.org/10.1016/j.est.2023.109219.

26) N.S. Dhaidan, M.S.M. Al-Jethelah, 12th IIR Conference Orford , Canada . May 21-23 (2018) 240-47. http://dx.doi.org/10.18462/iir.pcm.2018.0033

27) F.L. Rashid, N.S. Dhaidan, A.J. Mahdi, S.A. Kadhim, K.A. Hammoodi, M.A. Al-Obaidi, H.I. Mohammed, S. Ahmad, S. Salahshour, E.B. Agyekum, Int. Commun. Heat Mass Transf. 162, (2025) 108573. https://doi.org/10.1016/j.icheatmasstransfer.2024.108573.

28) A.M. Ahangar, A. Rahmani, M. Maleki, R. Ahmadi, S.H. Razavi, Sol. Energy Mater. Sol. Cells. 277 (2024) 113084. https://doi.org/10.1016/j.solmat.2024.113084.

29) F.L. Rashid, N.S. Dhaidan, A.J. Mahdi, H.N. Azziz, R. Parveen, H. Togun, R.Z. Homod, Int. Commun. Heat Mass Transf. 159 (2024) 108096. https://doi.org/10.1016/j.icheatmasstransfer.2024.108096.

30) A. NematpourKeshteli, M. Iasiello, G. Langella, N. Bianco, Therm. Sci. Eng. Prog. 52 (2024) 102690. https://doi.org/10.1016/j.tsep.2024.102690.

31) S. Ganapathiraman, P. Manickam, J. Energy Storage. 84 (2024) 110929. https://doi.org/10.1016/j.est.2024.110929.

32) A. Uniyal, Y.K. Prajapati, D. Kumar, Appl. Energy. 377 (2025) 124501. https://doi.org/10.1016/j.apenergy.2024.124501.

Figure captions

Figure.1 Experimental setup (a) Schematic diagram (b) Front view and top view the ETC (c) photographic view

Figure.2 DSC graph of the Latent Heat materials (a) Candilliea wax (b) Rice bran wax

Figure.3 Variation of ETC system parameters at air velocity of 15 m/s (a) Different temperatures and solar intensity Vs Time (b) Efficiency and solar intensity Vs Time

Figure.4 Variation of ETC system parameters at air velocity of 20 m/s (a) Different temperatures and solar intensity Vs Time (b) Efficiency and solar intensity Vs Time

Figure.5 Variation of ETC system parameters at air velocity of 25 m/s (a) Different temperatures and solar intensity Vs Time (b) Efficiency and solar intensity Vs Time

Table 1 Details about the Solar Air heater Collector and Sensible Heat storage materials

Specification of Collector Tubes	**Values**
Total length	1800 mm
Inner length	1760 mm
Coating length	1720 mm
Inner diameter	44 mm
Outer diameter	58 mm
Properties of used Engine oil (SAE 20W- 40)	
Kinematic viscosity @ 100 ^{0}C, cst	12.5-14.5
Flash point coc, ^{0}C, min	198
Pour point C, max	-19
Viscosity index	102
Copper strip corrosion 3 h @ 100 _C (astm), max	1.0
Neutralisation number mg koh/g, max	5.8
250 ^{0}C	5.6
280 ^{0}C	5.4
300 ^{0}C	5.2

Table 2 Details about Latent Heat storage materials

Properties of RBX wax	**Values**
Melting point	76.05 ^{0}C
Specific heat	2.11 kJ/kg ^{0}C
Latent heat of fusion	190.6 kJ/kg
Thermal conductivity	0.219 (solid) (W/m K)
Density at 70 ^{0}C	0.821 kg/m^3
Properties of CLX wax	
Melting point	66.6 ^{0}C
Specific heat	1.98 kJ/kg ^{0}C
Latent heat of fusion	129.7 kJ/kg
Thermal conductivity	0.198 (solid) (W/m K)
Density at 70 ^{0}C	0.784 kg/m^3

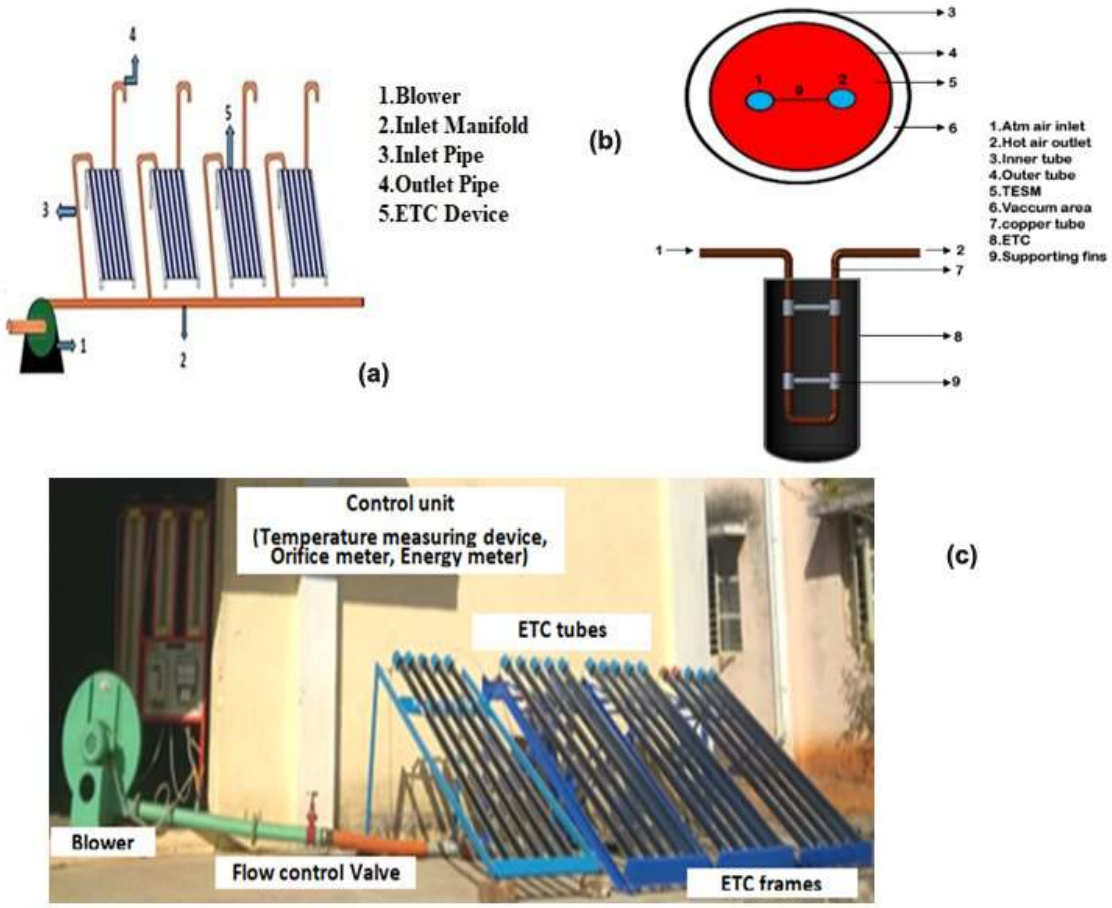
1.Blower
2.Inlet Manifold
3.Inlet Pipe
4.Outlet Pipe
5.ETC Device
(a)
(b)
1.Atm air inlet
2.Hot air outlet
3.Inner tube
4.Outer tube
5.TESM
6.Vaccum area
7.copper tube
8.ETC
9.Supporting fins
Control unit
(Temperature measuring device, Orifice meter, Energy meter)
ETC tubes
Blower
Flow control Valve
ETC frames
(c)

Figure.1

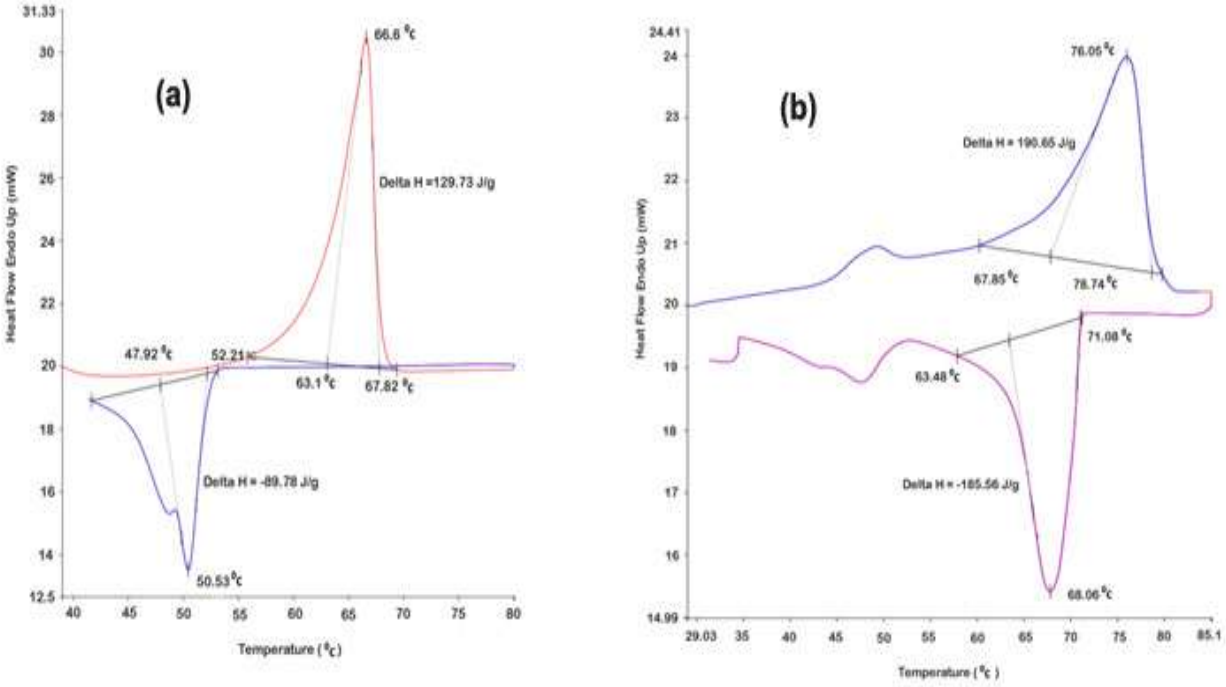
(a)
66.6 °c
Delta H =129.73 J/g
47.92 °c
52.21 °c
63.1 °c
67.82 °c
Delta H = -89.78 J/g
50.53 °c
Heat Flow Endo Up (mW)
Temperature (°c)
(b)
76.05 °c
Delta H = 190.65 J/g
67.85 °c
78.74 °c
71.08 °c
63.48 °c
Delta H = -185.56 J/g
68.06 °c
Heat Flow Endo Up (mW)
Temperature (°c)

Figure.2

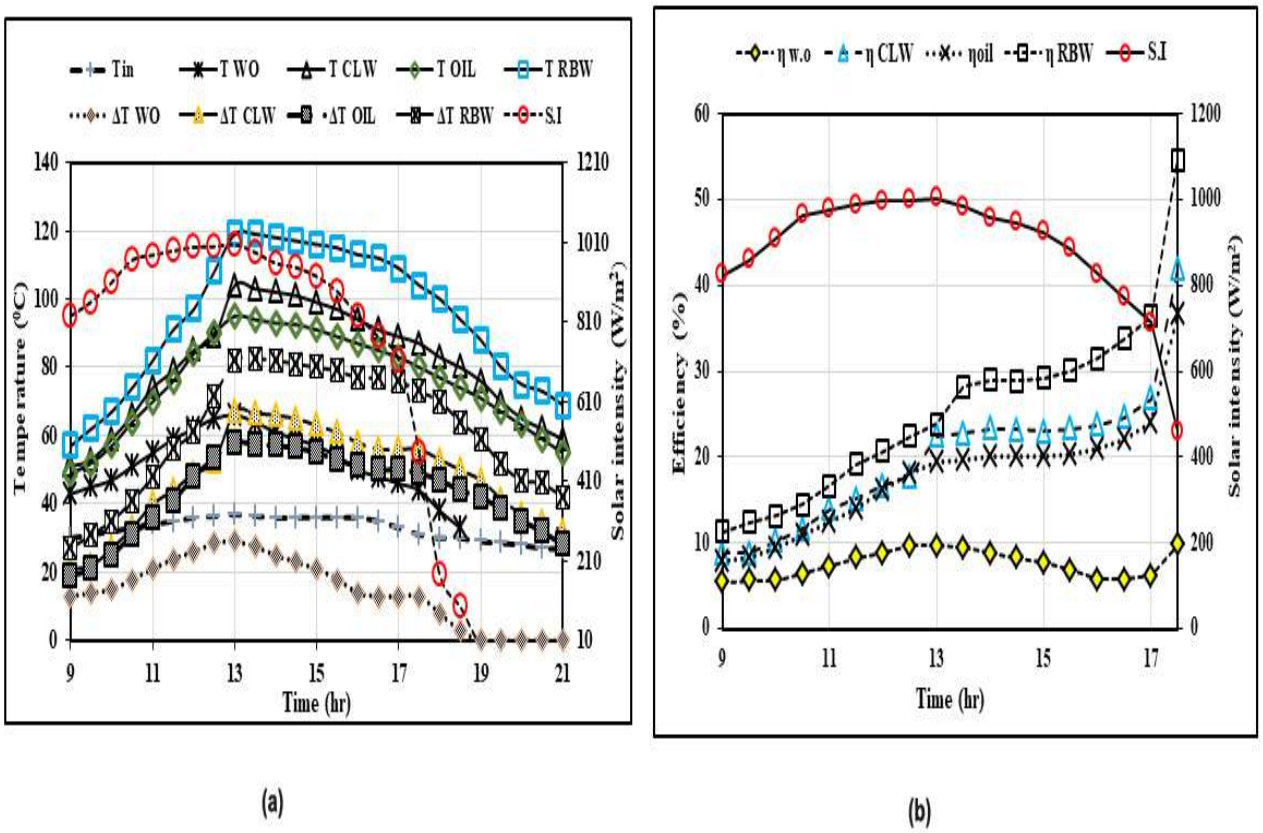
Tin
T WO
T CLW
T OIL
T RBW
ΔT WO
ΔT CLW
ΔT OIL
ΔT RBW
S.I
Temperature (°C)
Solar intensity (W/m²)
Time (hr)
(a)
ηw.o
ηCLW
ηoil
ηRBW
S.I
Efficiency (%)
Solar intensity (W/m²)
Time (hr)
(b)

Figure.3

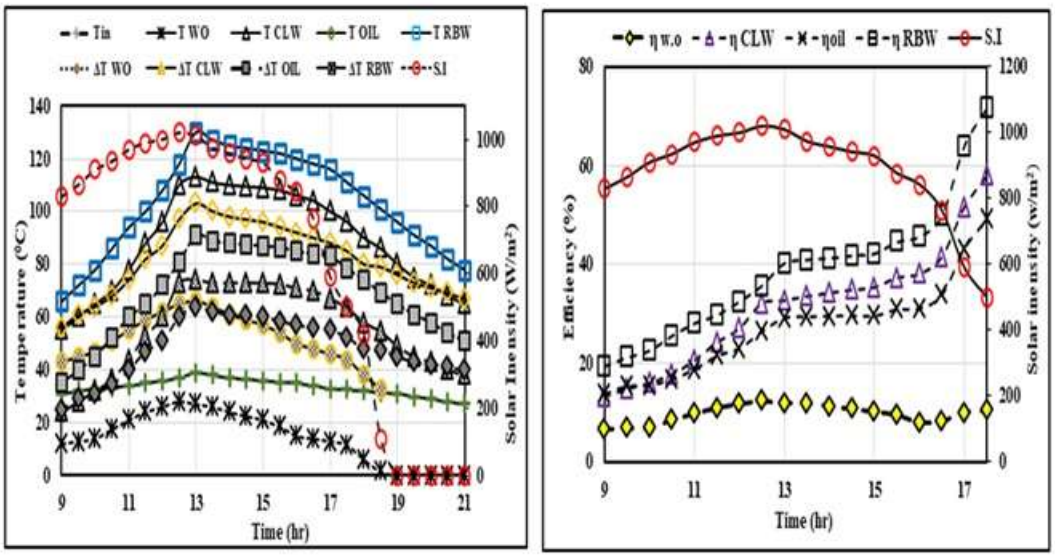
Tin
T WO
T CLW
T OIL
T RBW
ΔT WO
ΔT CLW
ΔT OIL
ΔT RBW
S.I
Temperature (°C)
Solar Inensity (W/m²)
Time (hr)
η w.o
η CLW
ηoil
η RBW
S.I
Efficiency (%)
Solar inensity (w/m²)
Time (hr)

Figure.4

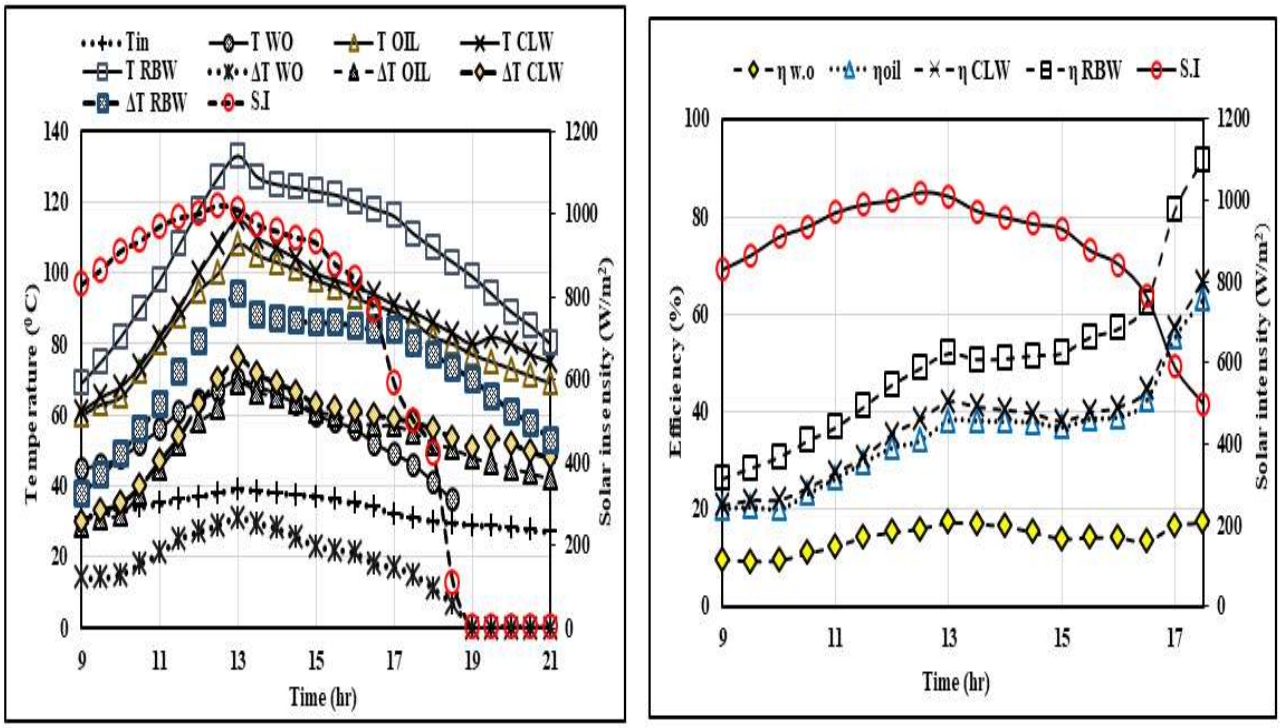
Tin
T WO
T OIL
T CLW
T RBW
ΔT WO
ΔT OIL
ΔT CLW
ΔT RBW
S.I
Temperature (°C)
Solar insensity (W/m²)
Time (hr)
(a)
η w.o
ηoil
η CLW
η RBW
S.I
Efficiency (%)
Solar intensity (W/m²)
Time (hr)
(b)

Figure.5